АСТРОФИЗИКА

ТОМ 65 МАЙ, 2022 ВЫПУСК 2

DOI: 10.54503/0571-7132-2022.65.2-2

ANALYSIS OF EMISSION LINE WIDTHS OF [CII] 158 μm

A.L.SAMSONYAN

Received 23 February 2022
Accepted 3 May 2022

A study of [CII] 158 μm emission line profiles observed with Herschel PACS for 379 galaxies is presented. Emission line widths are compared to [CII] luminosities, to near-infrared 1.6 μm luminosities and to infrared 22 μm luminosities to decide if any luminosity relates to velocity dispersion. Archival data for [CII] fluxes and line profiles are taken from http://cassis.sirtf.com/herschel/. Line profiles are classified as Gaussian, flattened and asymmetric. H magnitudes are taken from 2MASS catalogues, and 22 μm fluxes from the WISE catalogue. These luminosities are compared to [CII] line Full Width Half Maximum. Asymmetric profiles are not primarily AGN, which indicates that asymmetries are not produced primarily by outflows from the nuclear region. [CII] line widths do not show a significant correlation with any measure of galaxy luminosity. The correlation having smallest dispersion is with the H band luminosity for which $L(H) \sim FWHM^{0.73}$, which is a much flatter correlation than the $L \sim FWHM^4$ previously found for optical emission lines or stellar velocity dispersions.

Keywords: *infrared: galaxies - galaxies: starburst - galaxies: active - galaxies: distances and redshifts*

1. *Introduction*. Investigation of early galaxies is crucial for understanding galaxy formation and evolution. A particularly important new capability is the study of the far infrared [CII] 158 μm emission line. Especially in dusty, obscured sources it may be the only line observable with currently available techniques.

This [CII] line is the strongest far-infrared line in most sources [1-5] and is associated with star formation because it arises within the photodissociation region (PDR) surrounding starbursts [6-9]. Numerous observations of the [CII] line have been made [10-15] using the Photodetector Array Camera and Spectrometer (PACS) instrument [16] on the Herschel Space Observatory [17]. The [CII] line profiles are often of very high quality, with velocity resolution $<250\,km\,s^{-1}$, so the line profiles themselves potentially contain diagnostic information.

In previous papers [18,13], we compared the [CII] line with mid-infrared emission lines and with the Polycyclic Aromatic Hydrocarbon (PAH) feature observed with the Infrared Spectrograph (IRS; [19]) on the Spitzer Space Telescope [20]. These comparisons led to our calibration of the star formation rate (SFR) based on [CII] luminosities such that $\log SFR = \log L([CII]) - 7.0$ for SFR in solar masses/year and L([CII]) in solar luminosities. For those sources also observed

at high resolution with the IRS, we compared line widths for various emission lines and confirmed the association of [CII] with the starburst component of 379 sources ([21], hereafter S16). The [CII] line profiles were published in S16. In this paper our primary new results are a classification of the line profiles based on shape, and comparisons of the line widths with various other properties of the galaxies to search for astrophysical mechanisms that control the line widths.

2. *Sample selection and data*. For the analysis in this paper, the [CII] profiles shown in S16 are used. These profiles arise from the 8" x 8" spaxel of the PACS observation which is most closely aligned with the position of the Spitzer IRS observations used for comparisons in S16. All data used for the analysis in section 3 are available in VizieR Online Data Catalog. Table 1 lists some objects as an example from the catalog. In the columns of Table 1 are sequentially given: 1) name of objects, 2) luminosity distance in Mpc determined using redshift if $z > 0.01$ with $H_0 = 71$ km/s/Mpc, $\Omega_M = 0.27$ and $\Omega_\Lambda = 0.73$, from

Table 1

DATA SOURCES IN FIGURES. COMPLETE LIST IS IN VizieR ONLINE DATA CATALOG

Object Name	D	FWHM	Classification	Size	L([CII])	H	L(H)	22 μm	L(22) μm
1	2	3	4	5	6	7	8	9	10
Mrk0334	95.2	249	g	3.46	7.90	11.1	10.29	2.46	10.52
NGC0023	64.6	386	g	2.38	7.96	9.3	10.67	2.50	10.16
NGC34/mkn938	83.3	364	g	3.04	7.84	10.5	10.38	1.72	10.7
MCG-02-01-051/2	118	197	g	4.23	8.24	11.8	10.19	2.38	10.73
IRAS00188-0856	596	310	g	17.74	8.26	14.0	10.72	4.32	11.37
IRAS00199-7426	436	269	g	13.76	8.67	13.2	10.77	4.06	11.2
Haro 11	88.9	157	g	3.24	7.83	12.4	9.71	1.48	10.85
NGC185	0.72	47	g	0.03	2.34	7.1	7.63	7.54	4.25
E12-G21	143	333	g	5.08	8.14	11.3	10.57	3.95	10.28
IRAS00397-1312	1317			31.38	8.17	15.5	10.80	4.61	11.94
NGC0232a	98.4	449	g	3.57	8.23	10.3	10.62	2.54	10.51
NGC0232b	95.8	499	g	3.48	6.85	10.5	10.52	3.33	10.18
NGC253	3.24	67	g	0.12	5.84	4.1	10.13	-2.66	9.63
IZW1	271	310	g	9.12	7.85	11.2	11.15	2.37	11.46
MCG+12-02-001	68.8	106	g	2.53	7.86	10.9	10.07	1.19	10.74
NGC0317B	72.5	399	g	2.66	7.85	11.9	9.73	2.60	10.23
ESO541-IG12	250	340	g	8.49	7.69	11.9	10.81	3.47	10.95
IRAS01003-2238	542	100	g	16.47	8.01	15.3	10.12	3.10	11.77
3C31	72.5	699	f	2.66	6.69	8.9	10.92	6.44	8.69
3C120	145.2	289	a	5.16	7.51	11.09	10.65	2.883	10.71
Arp193	100.7	391	a	3.65	8.37	11.45	10.19	2.379	10.6
NGC7603	127.1	398	f	4.55	7.66	9.958	10.99	3.356	10.41

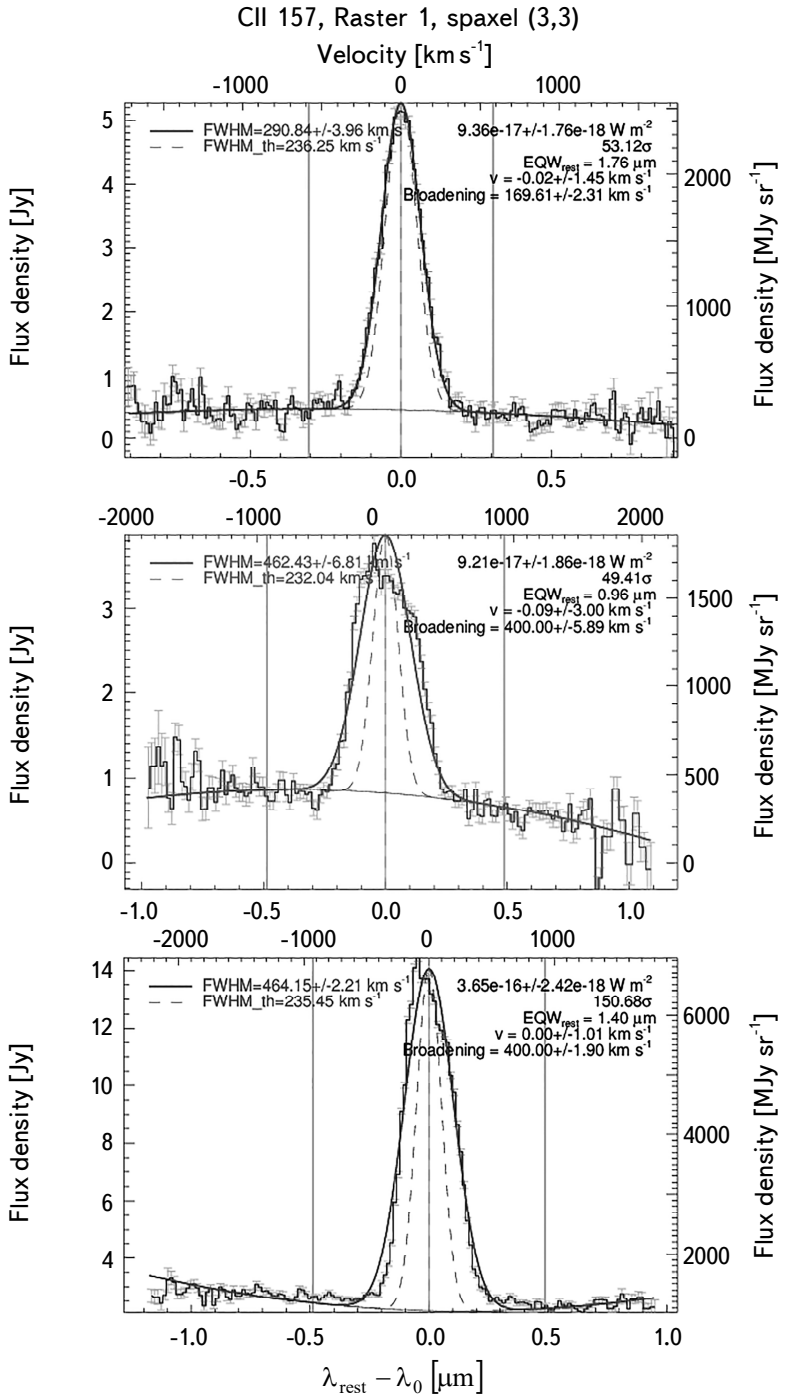

Fig.1. Examples of profile classifications as Gaussian (top, NGC3393), flattened (center, NGC7603), and asymmetric (bottom, ESO323-G077) as listed in Table 1. All profiles used are shown in http://cassis.sirtf.com/herschel/.

[24]. If the redshift is <0.01, redshift-independent distances from NASA Extragalactic Database are used. 3) FWHM of [CII] emission line profile shown in S16. Values of 100 are sources with observed FWHM less than instrumental resolution. 4) Classification of profile shape; "g" is Gaussian, "a" is asymmetric and "f" is flattened. Sources with missing classification are those with [CII] in limits, or very noisy profiles. 5) Projected size corresponding to 8 arcsec PACS spaxel. 6) Log of luminosity in solar luminosities of [CII] line using line flux from profiles in S16. 7) H band magnitude from 2MASS using Extended Sources Catalog and All-Sky Catalog for Point Sources. 8) H band luminosities νL_ν in solar luminosities using H magnitudes from 2MASS. 9) 22 μm (band 4) magnitude from AllWISE Data Release. 10) 22 μm luminosity νL in solar luminosities using WISE 22 μm magnitudes. The full table is available online in VizieR lists all sources with the same numbering and naming conventions as in S16; coordinates, observation numbers, and other ancillary data are in S16.

The [CII] results in Table 1 are some of the profile classifications with examples in Fig.1, the full list of the FWHM of the profile from the Gaussian fits illustrated in http://cassis.sirtf.com/herschel/(profiles and profile data are in the EPS column under "Line Profile"), and the luminosities of the [CII] line derived from the fluxes shown in the profiles. The FWHM-s listed are intrinsic widths, after correcting for instrumental resolution of 236 km/s. The FWHM errors are also given in the webpage, the errors are so small, that they can be neglected. Archival data for H band fluxes and luminosities from the Two Micron All Sky Survey (2MASS; [22]) and for 22 μm fluxes and luminosities from the Wide-Field Infrared Survey Explorer (WISE; [23]) are also given.

For use in the present paper, I have classified all of the [CII] profiles by shape, as compared to the best fitted Gaussian profiles illustrated in S16. The objective of this classification is to distinguish among profiles obviously affected by disk rotation and those profiles which probably arise because of virialized three dimensional motions of the gas. Flattened profiles are those which have the clearest evidence of velocities dominated by rotation. Asymmetric profiles show evidence either of systematic gas outflows, or of rotation by an inhomogeneous disk.

3. *Analysis and discussion*. The objective of this study is to search for what physical characteristic of the galaxies is primarily responsible for determining the observed [CII] profile widths. Much of the analysis in S16 was designed to compare the [CII] line to mid-infrared forbidden lines observed with the Spitzer IRS, with the goal of seeking differences between AGN and starburst sources. As described and reviewed in that paper, the mid-infrared AGN/starburst classification is made using the strength relative to continuum (equivalent width - EW) of the 6.2 μm PAH emission feature. In Fig.2, the [CII] line widths are seen to be

independent of this classification, as also shown in S16.

The new result in Fig.2 is including the classification of profile shapes. One notable conclusion is that the asymmetric and flattened profiles are generally broader. This indicates that profiles with evidence of rotation generally show higher velocities. This is expected from dynamics of disk rotation compared to three dimensional velocity dispersions arising within a galactic bulge, as pointed out for example by Nelson & Whittle [25]. The rotational velocity of the disk represents the potential of the disk and halo, yielding V_{max} expected to be about 1.5 times the dispersion within the bulge. That flattened profiles are broader is evidence that the classification of profiles has a meaningful physical interpretation and leads to the comparisons below that use only Gaussian profiles for considering which galactic properties might control these velocity dispersions. Another important conclusion from Fig.2 is that the asymmetric profiles are not primarily AGN, which implies the asymmetries are not produced primarily by outflows from the nuclear region.

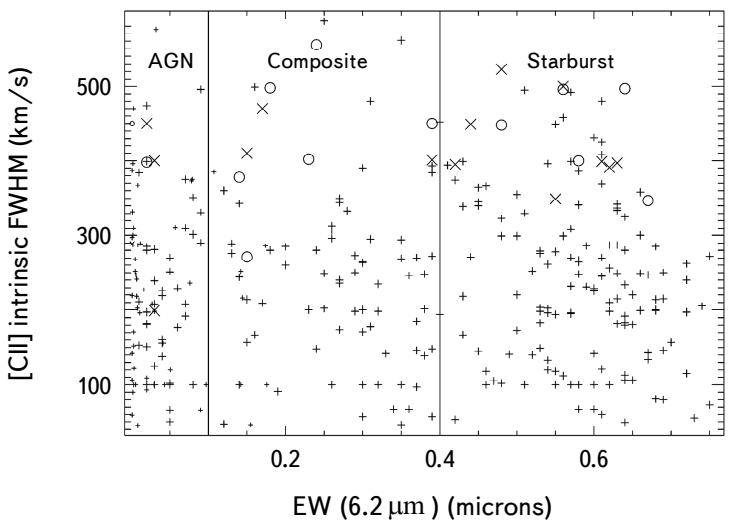

Fig.2. Profile FWHM compared to AGN/Starburst classification showing Gaussian profiles (+), asymmetric profiles (X) and flattened profiles (O). Horizontal axis shows the classification of sources using the 6.2 μm PAH feature; AGN have EW(6.2 μm)<0.1 μm , Composite (AGN plus starburst) have 0.1 μm <W(6.2 μm)<0.4 μm , and starbursts have EW(6.2 μm) > 0.4 μm .

Fig.3 shows the comparison of luminosities to sizes. The luminosities of the [CII] sources in Table 1 are for a single PACS spaxel. Transforming the 8" spaxel to a physical size gives the values in Table 1, which are plotted in Fig.3. The [CII] luminosities for the local sources level off for sizes > 8 kpc, indicating that most luminosity arises with this area. This is also an appropriate size to adopt for a galactic bulge, so the kinematical analysis below for the FWHM will be restricted to sources

of size < 8 kpc. If more details are desired of galaxy morphologies, optical images of individual sources can be seen with overlays showing the PACS spaxels in the "footprint" column of http://cassis.sirtf.com/herschel/.

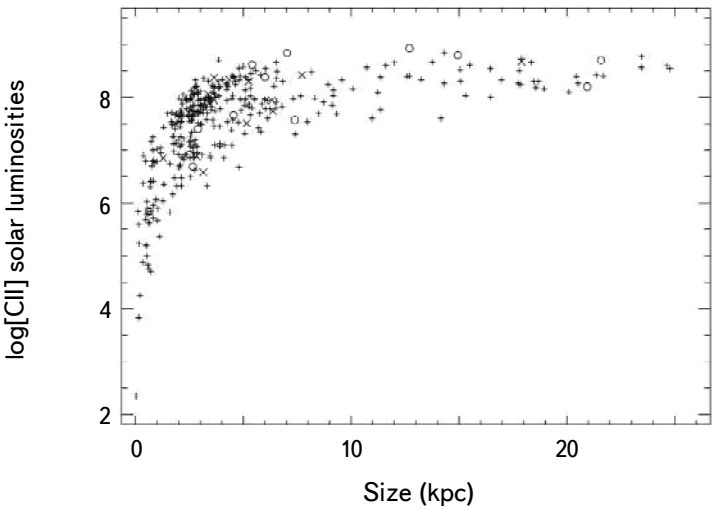

Fig.3. [CII] luminosities compared to observed size. Symbols are as in Fig.2.

The second objective of this paper is to compare [CII] FWHM to other galactic parameters in search of correlations. It has long been known that stellar velocity dispersions within galactic bulges relate to bulge luminosity with a form $L \propto \sigma n$ for σ the stellar line of sight velocity dispersion. This relates to the FWHM by $FWHM = 2.35\sigma$, and FWHM is normally used as the measure of velocity dispersion when using optical emission lines [26-28]. The initial study [29] found that $3 < n < 4$. In a reevaluation of a large sample of galactic bulges, Whittle [27] found $n = 3.2$. When using the [OIII] optical emission line, primarily for Seyfert galaxies, he found $n = 2.2$. Subsequent studies by Nelson & Whittle [25] and Shields et al. [28] determined that even the [OIII] widths from the narrow line region of AGN are controlled primarily by bulge gravity rather than by other sources inputing kinetic energy to the gas. More recent studies of relations between velocity dispersions and bulge gravity emphasized the use of sigma to determine relations among the masses of central black holes, bulge velocity dispersions, and bulge luminosities. The comprehensive summary of Kormendy & Ho studies [30] yields $n = 3.7$, and that of McConnell & Ma [31] gives $n = 5.1$.

Based on this extensive previous work, it would be expected that any integrated measure of velocity dispersion for a galaxy should show a meaningful correlation with the mass of that galaxy. This is my motive for comparing the FWHM of the [CII] lines with three different measures of galaxy luminosity, each of which

measures a different mass. The three parameters are: 1. the luminosity of the [CII] line itself, which scales primarily with the photodissociation regions surrounding starbursts and so scales with the gas mass connected to star formation; 2. The luminosity of dust reradiation, taken as 22 μm dust luminosity, which scales with the total luminosity of younger, hotter stars that are heating the dust; 3. The near infrared (H band) luminosity of the galaxy, which scales with the total luminosity of the evolved stars. Comparisons of [CII] FWHM with these three measures of luminosity are shown in Fig.4 and 5. These plots include only sources in Table 1 with Gaussian profiles, and only objects with size <8 kpc. This gives more confidence that the observed FWHM represent velocity dispersions that measure gravity from the halo regions of the galaxies.

Fig.4 illustrates the results using the conventional comparison of logL with logFWHM. In all cases, the value of n is much smaller than previous studies using stellar velocity dispersions or optical emission lines. For [CII] luminosities, $n = 1.52 \pm 0.24$; for 22 μm luminosities, $n = 0.38 \pm 0.20$; for H luminosities, $n = 0.73 \pm 0.11$.

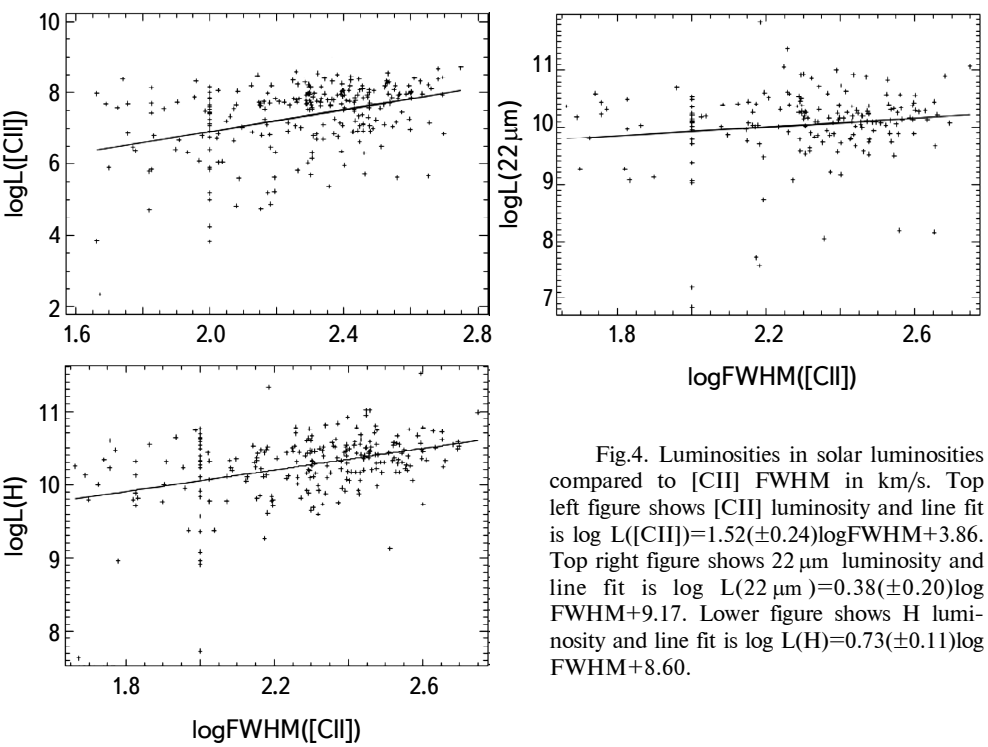

Fig.4. Luminosities in solar luminosities compared to [CII] FWHM in km/s. Top left figure shows [CII] luminosity and line fit is log L([CII])=1.52(±0.24)logFWHM+3.86. Top right figure shows 22 μm luminosity and line fit is log L(22 μm)=0.38(±0.20)log FWHM+9.17. Lower figure shows H luminosity and line fit is log L(H)=0.73(±0.11)log FWHM+8.60.

In Fig.5, the fits are shown using linear values for FWHM to compare scatter among the comparisons using the different parameters. These plots show the scatter in the luminosity distributions above and below the formal fits ($\pm 1\sigma$ for logL) within three different ranges of FWHM. In all cases, the scatter is extreme. The

range of luminosities at a given value of FWHM is comparable in all cases to the full range of FWHM over all luminosities. There can be a factor of 5 range in gas velocities for the same value of luminosity. It does not appear, therefore, that FWHM for [CII] can be used in a meaningful way to predict any kind of galaxy luminosity.

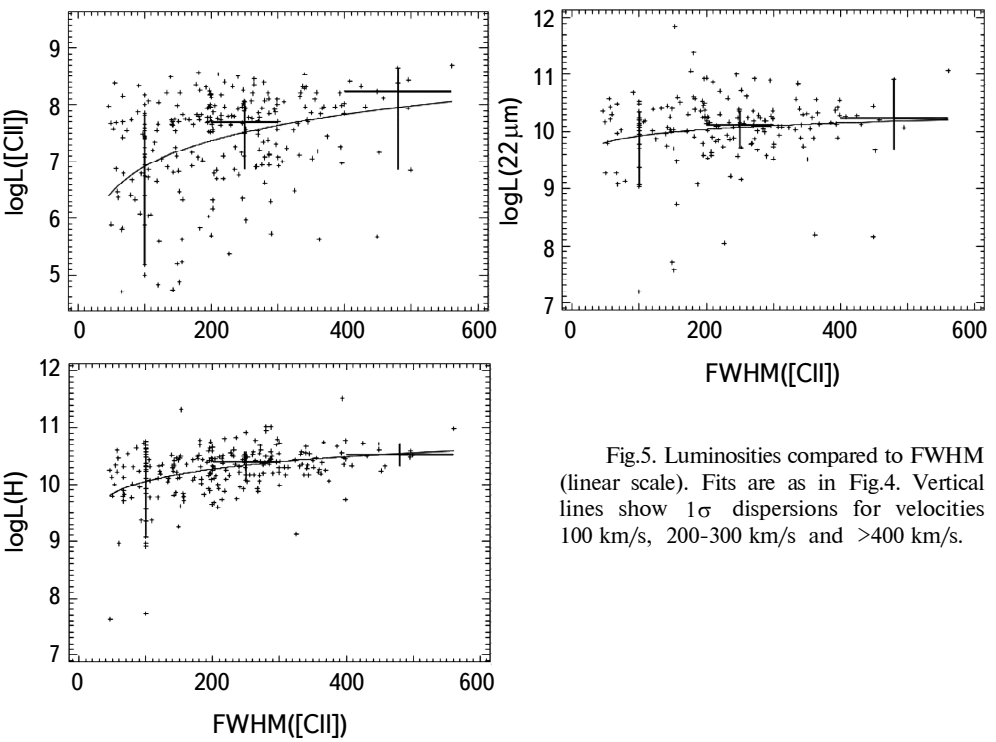

Fig.5. Luminosities compared to FWHM (linear scale). Fits are as in Fig.4. Vertical lines show 1σ dispersions for velocities 100 km/s, 200-300 km/s and >400 km/s.

Despite the large scatters, the results do imply a meaningful conclusion. The luminosity dispersions are smallest for the H band luminosities, next for the dust luminosities, and largest for the [CII] luminosities. This scaling of luminosity dispersions also progresses the same as the uncertainties in the slopes of the line fits in Fig.4 (smallest uncertainty for H luminosity). In both cases, therefore, the correlation of FWHM with H band luminosity is better than with either other parameter. I conclude from this that the gravity associated with the mass of evolved stars is a factor controlling the widths of the [CII] line. Nevertheless, the large range in gas velocities that can be found at the same value of luminosity remains puzzling. It seems that some unidentified process other than straightforward gravitational forces within the galactic bulge is the primary controller of CII gas velocities.

4. *Summary*. I classify [CII] 158 μm profiles for 379 galaxies observed with Herschel PACS as Gaussian, flattened and asymmetric based on the comparison

of observed profiles to Gaussian fits. Profile shapes can indicate the origin of the line widths because the lines whose width is caused by three dimensional random motions in a galaxy should be Gaussian, but widths caused by rotation of a disk should not be Gaussian. Emission line widths are compared to [CII] luminosities, to near-infrared 1.6 μm luminosities and to infrared 22 μm luminosities to decide if any luminosity accurately relates to velocity dispersion. The luminosity dispersions are smallest for H band luminosities and the slope uncertainty for the line fit is the smallest for H luminosities. I conclude from this that the gravity associated with the mass of evolved stars is a weak factor controlling the widths of the [CII] line, but line widths are primarily determined by a mechanism that is still unknown.

Acknowledgements. This work was made possible by a research grant number № 21AG-1C044 from Science Committee of Ministry of Education, Science, Culture and Sports RA.

I express great appreciation to those who developed the missions responsible for the archival data used in this paper: the PACS instrument on the Herschel Space Observatory, the IRS instrument on the Spitzer Space Telescope, the 2MASS Survey, and the WISE survey. These all are unique databases that may never be improved by future projects. I also thank my colleagues who initially involved me in research with the IRS and PACS: Lusine Sargsyan, Daniel Weedman, Vianney Lebouteiller, Don Barry and James Houck.

V.A.Ambartsumian Byurakan Astrophysical Observatory (BAO),
Armenia, e-mail: anahit.sam@gmail.com

АНАЛИЗЫ ПОЛУШИРИНЫ ЭМИССИОННОЙ ЛИНИИ [CII] 158 мкм

А.Л.САМСОНЯН

В работе представлено исследование профилей эмиссионной линии [CII]158 мкм для 379 галактик, наблюдаемых с помощью инструмента PACS космической обсерватории Гершель. Полуширины эмиссионных линий были сравнены со светимостью в ближней инфракрасной области 1.6 мкм и со светимостью в инфракрасной области 22 мкм, чтобы понять - связана ли какая-либо светимость с дисперсией скоростей. Архивные данные для потоков [CII] и профилей линий взяты с http://cassis.sirtf.com/herschel/. Профили линий

классифицированы как гауссовские, но уплощенные и асимметричные. H величины взяты из каталогов 2MASS, а 22 мкм потоки взяты из каталога WISE. Эти светимости сравнены с полушириной линии [CII]. Асимметричные профили не являются АЯГ-ами (Активное Ядро Галактики), что указывает на то, что асимметрии в линиях не являются последствием оттока из ядерной области. Ширина линий [CII] не показывает значительной корреляции с какой-либо мерой светимости галактик. Корреляция с наименьшей дисперсией показывает светимость в H диапазоне, для которого $L(H) \sim FWHM^{0.73}$, что является гораздо более плоской корреляцией, чем $L \sim FWHM^4$, полученная ранее для оптических линий излучения или дисперсий звездных скоростей.

Ключевые слова: *инфракрасный:галактики - галактики звездообразования: галактики - активные: расстояния и красные смещения*

REFERENCES

1. *G.J.Stacey*, *N.Geis*, *R.Genzel et al.*, Astrophys. J., **373**, 423, 1991.
2. *S.Malhotra*, *G.Helou*, *G.Stacey et al.*, Astrophys. J., **491**, L27, 1997.
3. *T.Nikola*, *R.Genzel*, *F.Herrmann et al.*, Astrophys. J., **504**, 749, 1998.
4. *M.L.Luhman*, *S.Satyapal*, *J.Fischer et al.*, Astrophys. J., **594**, 758, 2003.
5. *J.R.Brauher*, *D.A.Dale*, *G.Helou*, Astrophys. J. Suppl. Ser., **178**, 280, 2008.
6. *A.G.G.M.Tielens*, *D.Hollenbach*, Astrophys. J., **291**, 722, 1985.
7. *G.Helou*, *S.Malhotra*, *D.J.Hollenbach et al.*, Astrophys. J., **548**, L73, 2001.
8. *S.Malhotra*, *M.J.Kaufman*, *D.Hollenbach et al.*, Astrophys. J., **561**, 766, 2001.
9. *R.Meijerink*, *M.Spaans*, *F.P.Israel*, Astron. Astrophys., **461**, 793, 2007.
10. *L.Sargsyan*, *V.Lebouteiller*, *D.Weedman et al.*, Astrophys. J., **755**, 171, 2012
11. *D.Farrah*, *V.Lebouteiller*, *H.W.W.Spoon et al.*, Astrophys. J., **776**, 38, 2013.
12. *T.Díaz-Santos*, *L.Armus*, *V.Charmandaris et al.*, Astrophys. J., **774**, 68, 2013.
13. *L.Sargsyan*, *A.Samsonyan*, *V.Lebouteiller et al.*, Astrophys. J., **790**, 15, 2014.
14. *I. De Looze*, *D.Cormier*, *V.Lebouteiller et al.*, Astron. Astrophys., **568**, A62, 2014.
15. *T.Díaz-Santos*, *L.Armus*, *V.Charmandaris et al.*, Astrophys. J., **788**, 17, 2014.
16. *A.Poglitsch*, *C.Waelkens*, *N.Geis et al.*, Astron. Astrophys., **518**, L2, 2010.
17. *G.L.Pilbratt*, *J.R.Riedinger*, *T.Passvogel et al.*, Astron. Astrophys., **518**, L1, 2010.
18. *L.Sargsyan*, *D.Weedman*, *V.Lebouteiller et al.*, Astrophys. J., **730**, 19, 2011.
19. *J.R.Houck*, *T.L.Roellig*, *J. van Cleve et al.*, Astrophys. J. Suppl. Ser., **154**, 18, 2004.
20. *M.W.Werner*, *T.L.Roellig*, *F.J.Low et al.*, Astrophys. J. Suppl. Ser., **154**, 1, 2004.
21. *A.Samsonyan*, *D.Weedman*, *V.Lebouteiller et al.*, Astrophys. J. Suppl. Ser., **226**, 11, 2016.

22. *M.F.Skrutskie*, *R.M.Cutri*, *R.Stiening et al.*, Astron. J., **131**, 1163, 2006.
23. *E.L.Wright*, *P.R.M.Eisenhardt*, *A.K.Mainzer et al.*, Astron. J., **140**, 1868, 2010.
24. *E.L.Wright*, Publ. Astron. Soc. Pacif., **118**, 1711, 2006.
25. *C.H.Nelson*, *M.Whittle*, Astrophys. J., **465**, 96, 1996.
26. *F.R.Feldman*, *D.W.Weedman*, *V.A.Balzano et al.*, Astrophys. J., **256**, 427, 1982.
27. *M.Whittle*, Astrophys. J., **387**, 121, 1992.
28. *G.A.Shields*, *K.Gebhardt*, *S.Salviander et al.*, Astrophys. J., **583**, 124, 2003.
29. *S.M.Faber*, *R.E.Jackson*, Astrophys. J., **204**, 668, 1976.
30. *J.Kormendy*, *L.C.Ho*, ARA&A, **51**, 511, 2013.
31. *N.J.McConnell*, *C.-P.Ma*, Astrophys. J., **764**, 184, 2013.